Laser-controlled microscale fluid flows near the air-liquid interface of suspension droplets

Kenji Miyakawa and Hiroto Adachi
Department of Applied Physics, Fukuoka University, Fukuoka 814-0180, Japan
(Received 28 April 2008; published 24 October 2008)

We investigate microscale flows of microparticles driven by a laser beam focused near the air-liquid interface of a suspension droplet. Three distinct regimes, convection, a linear flow, and a nonflow, are found by controlling both the position of the beam focus relative to the air-liquid interface and the laser power. They are governed by the most dominant of two effects exerted by a focused laser beam, i.e., local heating and radiation pressure. We find that in the nonflow regime two-dimensional close-packed arrays of microparticles are formed on the air-liquid interface, and spin on the beam axis. We show that micron-sized polystyrene beads can be bonded into a long chain structure by taking advantage of the linear flow.

DOI: 10.1103/PhysRevE.78.041407 PACS number(s): 82.70.Dd, 47.61.−k, 87.80.Cc, 83.10.Pp

I. INTRODUCTION

In a thin horizontal fluid layer with the free surface subjected to a vertical temperature gradient, convective motion arises above a critical applied temperature difference. This convection, called Marangoni-Bénard convection, is driven either by bulk forces arising from temperature-induced density differences (buoyancy) or by the surface force due to the heat-induced surface-tension differences (thermocapillarity) [1,2]. For small geometry and/or microgravity environments, the thermocapillary (or thermal Marangoni) effect is dominant, and flow along a liquid free surface arises. The thermal Marangoni effect has been successfully utilized in microscopic fluidic devices manipulating small quantities of fluid [3,4]. Recently, optical methods have been designed to impose thermal gradients, which is based on local heating induced by focusing light [5,6].

When a moderately powerful laser is focused close to the diffraction limit, a steep gradient in light intensity, in addition to a thermal gradient, is produced in the focal region. Small dielectric objects, such as polystyrene beads and silica microparticles, experience two forms of radiation pressure if its refractive index is higher than that of the surrounding medium. One is the force that tends to attract them to the high intensity region (gradient force). Another is the force that arises from reflection or absorption of light, and it tends to push microparticles along the beam, in the direction of propagation of the light (scattering force). Behaviors of microparticles are determined by a competition between effects of these forces [7,8]. If the effect of the gradient force is large enough to overcome the effect of the scattering force, microparticles are stably trapped in the focus position. To the contrary, if the effect of the scattering force is dominant, microparticles are pushed out from the focus position. It would be now interesting to induce a nonthermal flow of microparticles by utilizing these optical forces.

In this paper, we explore the possibility of optically driven microflows by focusing the laser light near the contact line of suspension droplets, liquid droplets containing a number of microparticles. We find three types of flow patterns governed by the contact angle of the droplet, convection, linear flow, and nonflow, when the position of the beam focus is fixed. We show that it is possible to assemble microparticles into a long chain, utilizing a linear flow being one of the resulting flows.

II. EXPERIMENT

We prepared suspensions of microparticles (particle density, 1.3×10^6 particles/mm^3) by dispersing polystyrene beads of 1 μm in diameter into distilled water. The solution of 2 μl was placed on the glass cover slip on the inverted microscope to form suspension droplets with the radius of about 3 mm, where the surface-treated cover slip (Matsunami, NEO) was used in preparation for droplets with high contact angles. In order to focus the laser beam near the air-liquid interface of the droplet, we used the optical trapping system. A circularly polarized Nd:YVO4 laser (Spectra-Physics, BL106C) operating at $\lambda=1064$ nm in a TEM_{00} mode was introduced into the inverted microscope (Nikon, TE300) and focused by the oil immersion objective lens (100×, NA=1.3). The microscope image was monitored by a charge coupled device (CCD) camera (chip size, 768 ×494 pixels) connected to the video recorder. In order to measure particle velocities up to 1 mm/s, we captured images at rates up to 1000FPS using a high-speed CCD camera (chip size, 640×480 pixels). A schematic diagram of the system is shown in Fig. 1. A small droplet on the glass cover slip is characterized by the contact angle θ_c and the height of

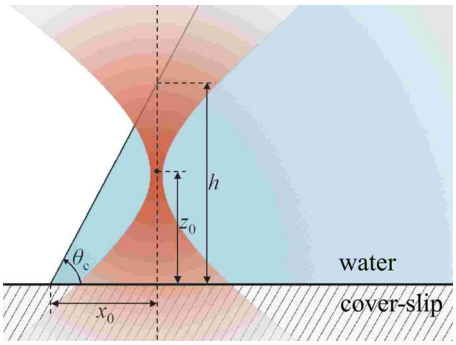

FIG. 1. (Color online) Schematic illustration of the experimental setup for optically driven flows, where (x_0, z_0), h, and θ_c denote the position of the beam focus, the thickness of the droplet along the optical axis, and the contact angle, respectively.

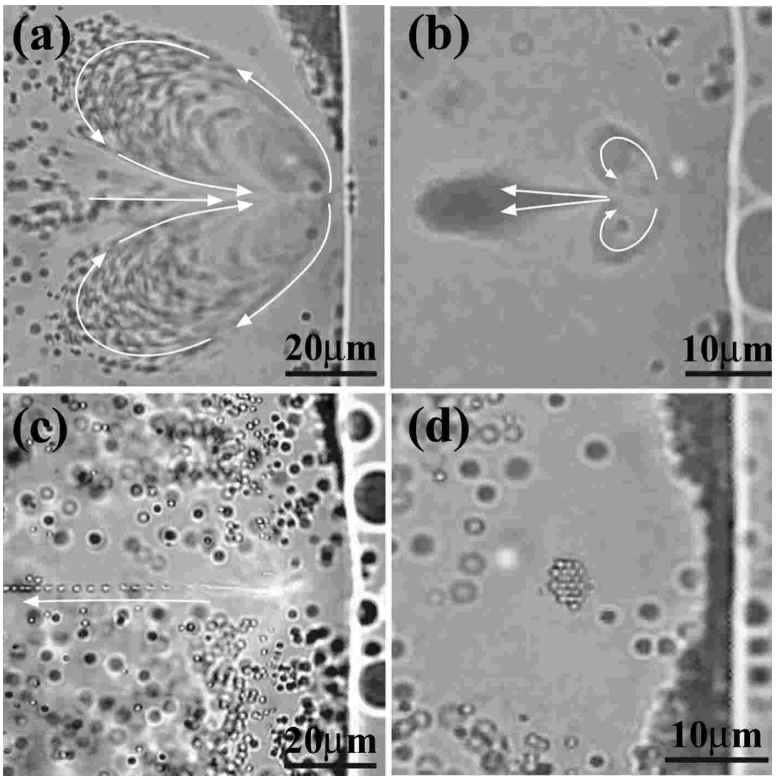

FIG. 2. Flow patterns of 1-μm-diameter polystyrene beads in the droplet with the contact angle θ_c, at the laser power of 200 mW; (a) $\theta_c=55°$ ($\Delta z \simeq 12.6$ μm), (b) $\theta_c=49°$ ($\Delta z \simeq 8$ μm), (c) $\theta_c=37°$ ($\Delta z \simeq 1.4$ μm), and (d) $\theta_c=21°$ ($\Delta z \simeq -4.6$ μm). Here the focal depth of the microscope is about 0.45 μm. The plane which is imaged by the microscope deviates from the focus position of the laser by about 1.5 μm, because of chromatic aberration. The arrows in each picture outline streamlines of particles. The longitudinal white line in each picture is the contact line of the droplet.

the droplet along the optical axis h. Here the desired θ_c was obtained by controlling the evaporation of a solvent. We specify the position of the beam focus by (x_0, z_0), where x_0 is the position of the optical axis relative to the contact line and z_0 is the focus position relative to the cover slip along the optical axis. In the experiment the focus position was fixed at $(x_0, z_0)=(16.5\ \mu\text{m}, 11.0\ \mu\text{m})$ by adjusting both the sample stage and the height of the objective lens. Here the focus position was measured with respect to air. Since the value of x_0 is very small compared with the droplet radius r, typically $x_0/r \sim 5.5\times10^{-3}$, h can be approximated as $h \simeq x_0 \tan\theta_c$. Then, the distance between the air-liquid interface and the point of the beam focus along the optical axis, Δz, which is a significant control parameter in this experiment, is given by $\Delta z = h - z_0$. Experiments were carried out at 21 °C ± 0.5 °C.

III. RESULTS AND DISCUSSION

When the contact angle of the droplet was varied, the resulting behaviors were roughly classified into three distinct types. Figure 2 shows typical patterns at the laser power of 200 mW. At $\theta_c=55°$ ($\Delta z \simeq 12.6$ μm), the flow with a butterflylike pattern appears, as shown in Fig. 2(a), where the blur inside the pattern is due to the relatively high particle velocity. As long as the laser power P was small, the fluid remained at rest. The fluid began to perform bulk movement organized in the butterflylike form when P exceeded a critical value of 150 mW. The particles flow along streamlines, as depicted by arrows in the figure. Let us consider the origin of this flow pattern. In general, in the beam waist of the laser, a fraction of the laser power is converted into heat. The increase in temperature within the focus is estimated to be a few K/W [9,10]. As long as the temperature increase is small, that is, the laser power is weak, the temperature increase is smeared by heat conduction only, which is not accompanied by a bulk motion of fluid.

From the observation that a bulk motion develops beyond a critical threshold, thermal convection seems the most likely candidate for the origin of the butterflylike motion. There is a possibility of evaporation, of course, as the different heat transport process is involved. However, this effect seems negligible, since every measurement was completed within 10 seconds after the beginning of laser illumination. The convective flow is probably driven by two effects. One is thermocapillarity as characterized by the Marangoni number $M=\sigma_T \Delta T d/\rho\nu\kappa$ in terms of the surface-tension temperature coefficient σ_T ($\equiv -d\sigma/dT > 0$), the liquid layer thickness d, the temperature difference across the liquid layer ΔT, the liquid density ρ, the kinematic viscosity ν, and the thermal diffusivity κ. The other is buoyancy as characterized by the Rayleigh number $R=g\alpha\Delta T d^3/\nu\kappa$ with the liquid thermal expansion coefficient α and the gravitational acceleration g. The ratio $M/R=\sigma_T/\rho\alpha g d^2$ characterizes the strength of thermocapillarity relative to buoyancy. $M/R > 1$ provides a necessary condition for thermocapillarity to dominate over buoyancy. Assuming that in our case d corresponds to Δz, the value of M/R is estimated to be about 4.8×10^5 (Table I). It follows from this that the observed flow would be governed by the Marangoni effect. The butterflylike pattern is characteristic of the convection driven by surface tension [11].

When $\theta_c=49°$ ($\Delta z \simeq 8$ μm), in addition to the butterflylike motion, a jetlike motion appeared, in which particles flow outward from the focus point [Fig. 2(b)]. Both motions occur in differently oriented planes, but the distance between such two planes is small. In addition, such a coexistence of

TABLE I. Values at 20 °C of physical properties of water for surface-tension-driven Bénard convection experiments.

Surface-tension coefficient σ_T	0.152×10^{-3} Nm^{-1} K^{-1}
Kinematic viscosity ν	1.00×10^{-6} m^2 s^{-1}
Thermal diffusivity κ	0.141×10^{-6} m^2 s^{-1}
Thermal expansion coefficient α	0.204×10^{-3} K^{-1}
Density ρ	0.998×10^{3} kg m^{-3}
Gravitational acceleration g	9.81 ms^{-2}

patterns was observed only in the very limited ranges of Δz and P. This behavior is considered to be a precursor of the transition to the next regime.

When $\Delta\theta_c=37°$, the focus position of the beam is almost at the air-water interface, i.e., $\Delta z\simeq1.4$ μm. At such small Δz, the butterflylike motion disappeared completely and a new pattern appeared steadily, in which particles flow only in a single direction, corresponding to the direction of propagation of the totally reflected light as described later, as shown in Fig. 2(c). The fashion of this flow, termed the linear flow, is entirely distinct from that of the butterflylike flow. The threshold power for the linear flow does not exist. These features suggest that the linear flow is not due to thermal convection. Instead, it is instructive to suppose that the linear flow is driven by radiation pressure. Let us consider the generation of the light flux propagating in the direction different from the incident direction of the light, with a geometrical ray optics analysis of a single light ray. Provided that the light ray reaches the interface between a denser medium with refractive index n_1 and a thinner medium with refractive index n_2 $(n_1>n_2)$, total internal reflection will occur at the interface for angles larger than the critical incident angle $\alpha_c=\sin^{-1}(n_2/n_1)$. In the case of the air-water interface, $\alpha_c=48.7°$ with $n_1=1.33$ and $n_2=1$. In our system, therefore, in which the Gaussian beam is focused on the air-water interface with the slope of 37° by the objective of the one-half angular aperture of about 60°, it is reasonable to suppose that a part of the beam will be totally reflected at the interface, as illustrated in Fig. 3. The width of the resulting reflected beam will be narrow, so that the effect of gradient force will be significantly small compared to the effect of the scattering force. Hence microparticles drawn to the focal point will be

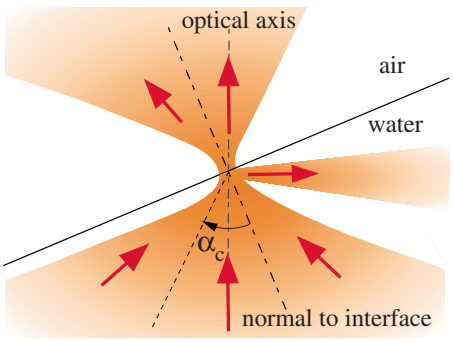

FIG. 3. (Color online) Schematic illustration of total internal reflection of the Gaussian beam focused on the air-water interface, where α_c is the critical incident angle.

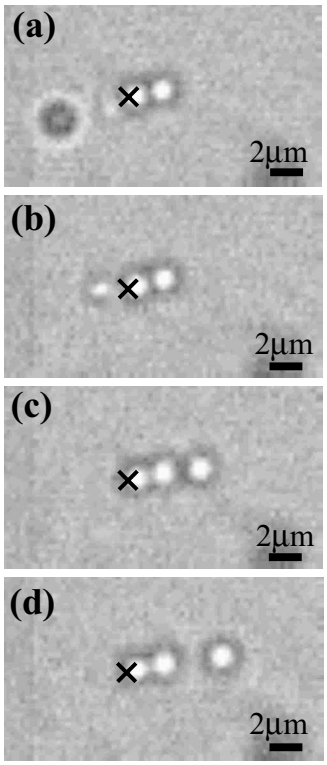

FIG. 4. Sequential images of the particle motion with the elapsed time t in the linear flow: (a) $t=0$, (b) $t=5$ ms, (c) $t=10$ ms, and (d) $t=15$ ms. The symbol (×) denotes the position of the beam focus.

pushed in the direction of propagation of the reflected beam. This is probably responsible for the linear flow of particles. The linear flow was observed, even if $\theta_c\geqq37°$, when the beam was focused on the air-water interface. On the other hand, the butterflylike pattern was not observed at $\theta_c=37°$, no matter where the focus position was.

Figure 4 shows sequential images of particles in the linear flow captured by the high-speed CCD camera. We see that a microparticle is drawn to the focal point and another microparticle is thereby pushed out from the focal point. Thus microparticles cannot be stably trapped in this focus position of the beam.

The width of the linear flow can be controlled by changing the focus position above the air-liquid interface, fixing x_0 at 16.5 μm and P at 200 mW. Figure 5 shows the width of the linear flow with a variation of Δz at $\theta_c=37°$. With bringing the focus position close to the air-liquid interface, the width of the flow monotonously decreases and finally comes to be of the order of the particle diameter. The flow width will be associated with the size of the totally reflected beam, and its size will be related to the size of the laser beam on the air-liquid interface. The size of the Gaussian beam w at the distance of Δz from the focus position is generally expressed as $w_0[1+(\Delta z/z_R)^2]^{1/2}$ with the beam waist w_0 and the Rayleigh length z_R [12]. We see that the Δz dependence of the observed flow width is in fair agreement with this expression, as shown by the dotted line in Fig. 5. This supports the view that a linear flow of microparticles is driven by the optical force.

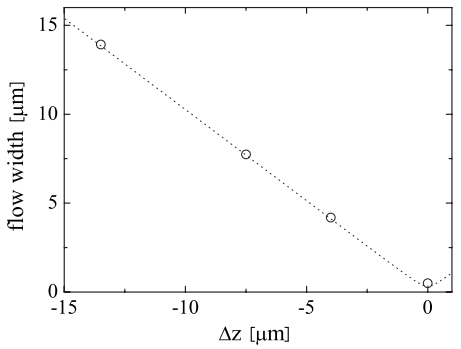

FIG. 5. Flow width as a function of Δz, the distance from the air-liquid interface along the optical axis. The dotted line shows the dependence of the diameter of the Gaussian beam on the distance Δz from the focal point. Here the widths of flow were measured as follows; first we captured the images of linear flow at various focus positions of the laser, measured the widths at 10 points along the flow using an image-processing software, and then averaged them.

When $\theta_c=21°$ ($\Delta z \simeq -4.6$ μm), any flow of particles did not appear, but beads were stably trapped in a two-dimensional (2D) array on the air-liquid interface, as shown in Fig. 2(d).

In this situation the position of the beam focus is above the air-liquid interface. Beads attracted to the focal point by the gradient force were pushed against the air-liquid interface, and were rearranged in the 2D array by the scattering forces. We attempted to trap seven beads into a close-packed array with a rotational symmetry by adjusting the height of the focus position, as shown in Fig. 6(a). A little more rise of the focus position caused such a 2D array to set in smooth rotation about the beam axis [Fig. 6(b)]. The sense and the rate of rotation depend on the handedness of the circular polarization and the power of the incident laser beam, respectively. Similar trapping and rotation of beads have been observed at the glass cover-slip–water interface in the cell consisting of two glass cover slips. These behaviors have been interpreted on the basis of the Fresnel diffraction of the focused Gaussian beam [13,14]. It should be noted that 2D trapping and rotation of microparticles are possible even on the soft interface such as the free interface. At $\theta_c \leqq 21°$, neither a butterflylike pattern nor a linear flow was observed, wherever the position of the beam focus.

The conditions determining which behavior of microparticles appears can be summarized with Δz and θ_c as follows.

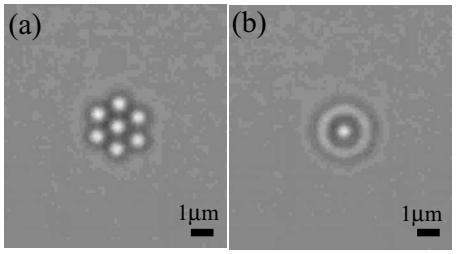

FIG. 6. Two-dimensional close-packed array of seven 1-μm-diameter polystyrene beads in the stationary state at $\Delta z = -1.0$ μm (a) and in the rotational state with the rate of 760 rpm at $\Delta z = -1.5$ μm (b).

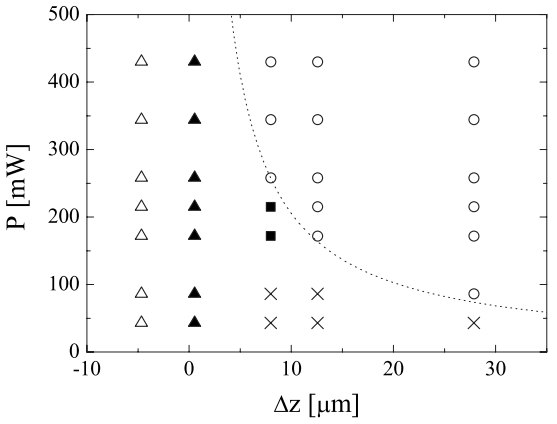

FIG. 7. Phase diagram in the plane of Δz and P. Symbols denote states of motions of particles: (○) convection, (■) a coexistence state of a convection and a linear flow, (▲) a linear flow, (△) a two-dimensional array, and (×) a stationary state.

For a butterflylike motion, Δz needs to be beyond 12.6 μm. For a linear flow, Δz needs to be nearly equal to zero and θ_c needs to be beyond 37°. For a two-dimensional trapping, Δz needs to be below zero and θ_c needs to be below 21°. Thus, we see that θ_c, in addition to Δz, is a significant control parameter for behaviors in which radiation pressure is involved. Figure 7 shows the phase diagram in the plane of Δz and P, where the position of the beam focus is fixed. One sees that the Δz-P plane is roughly divided into two regions; one is the region of large Δz in which the thermal Marangoni effect is dominant and the other is the region of small Δz in which the effect of radiation pressure is dominant. The boundary between both regions can be provided by evaluating the critical temperature deviation from ambient temperature $\Delta T_c = \rho \nu \kappa M_c / \sigma_T d$ as a function of Δz, using the critical Marangoni number M_c. Assuming that the temperature deviation from ambient temperature due to laser heating is proportional to the laser power, i.e., $\Delta T = \gamma P$ (γ, a constant) [15], the critical laser power P_c imposing the Marangoni convection can be expressed as $0.925 \times 10^{-6} M_c / \gamma d$ [W] using the values of physical parameters listed in Table I. Assuming that d corresponds to Δz, this expression represents nicely the boundary between convective and nonconvective regimes when $M_c / \gamma = 2.2$ W/K, as depicted by the dotted curve in Fig. 7.

We attempted to assemble polystyrene beads of 1 μm into a long chain in the suspension droplet, utilizing a linear flow. We added an aqueous solution of 0.3 μl of 30 mM $CaCl_2$ to a suspension droplet just before the beginning of laser irradiation, in order to enable beads to cause a face-to-face adhesion at the focal point. Figure 8 shows micrographs of sequential attachment with the elapsed time, where the assembly of beads grows along the flux of light being totally reflected at the air-liquid interface. Figure 8(e) shows a three-dimensional chain structure consisting of more than 1000 individual beads and the inset shows a close-up of the particle linkage. We see that single beads are stacked on the top of each other. Its binding is so robust as to hold a chain structure of the order of 1 mm. The stability and the structure

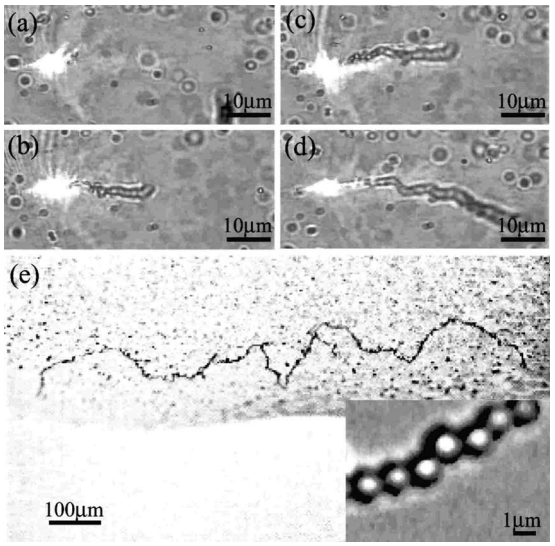

FIG. 8. Images of sequential attachment of beads with the elapsed time t in the linear flow: (a) $t=0$, (b) $t=1.5$ s, (c) $t=3.0$ s, (d) $t=4.5$ s, and (e) the fabricated chain of about 1.5 mm in length. The inset shows a close-up of bonding between particles. The bright spot in the left-hand part of (a)–(d) corresponds to the laser focus.

of the assembly are determined by an interplay among various factors; pair interactions between particles, the trapping potential of the focused laser, the pushing force of totally reflected light, and the Brownian motion of particles. It should be emphasized that fabricated chains are three-dimensionally suspended in the bulk solution, which differs from 2D laser-trapped structures adhered to substrates [16].

IV. CONCLUSION

We have experimentally investigated microscale flows in a suspension droplet driven by a focused laser beam. We have demonstrated three distinct regimes in behaviors of microparticles. One is the Marangoni convection induced by the effect of local heating of light, and the other two are the linear flow and 2D stationary trapping which are induced by the radiation pressure of light. We would like to emphasize that these behaviors are essentially determined by the position of the beam focus relative to the air-liquid interface. We have shown that microparticles can be assembled into chain structures by taking advantage of a linear flow. This method is applicable to not only transparent microparticles such as polystyrene beads but also nontransparent micro-objects that are difficult to optically trap, such as carbon nanotubes.

ACKNOWLEDGMENTS

This work was supported in part by a Grant-in-Aid for Scientific Research from the Ministry of Education, Culture, Sports, Science and Technology of Japan (Grants No. 15540377 and No. 18540385), and was also supported in part by the Central Research Institute of Fukuoka University.

[1] M. J. Block, Nature (London) **178**, 650 (1956).
[2] J. R. A. Pearson, J. Fluid Mech. **4**, 489 (1958).
[3] M. A. Burns, B. N. Johnson, S. N. Brahmasandra, K. Handique, J. R. Webster, M. Krishnan, T. S. Sammarco, P. M. Man, D. Jones, D. Heldsinger, C. H. Mastrangelo, and D. T. Burke, Science **282**, 484 (1998).
[4] D. E. Kataoka and S. M. Troian, Nature (London) **402**, 794 (1999).
[5] N. Garnier, R. O. Grigoriev, and M. F. Schatz, Phys. Rev. Lett. **91**, 054501 (2003).
[6] K. T. Kotz, K. A. Noble, and G. W. Faris, Appl. Phys. Lett. **85**, 2658 (2004).
[7] A. Ashkin, J. M. Dziedzic, J. E. Bjorkholm, and S. Chu, Opt. Lett. **11**, 288 (1986).
[8] A. Ashkin, J. M. Dziedzic, and T. Yamane, Nature (London) **330**, 769 (1987).
[9] S. M. Block, in *Noninvasive Techniques in Cell Biology*, edited by S. Grinstein and K. Foskett (Wiley-Liss, New York, 1990), pp. 375–401.
[10] S. Wurlitzer, C. Lautz, M. Liley, C. Duschl, and T. M. Fischer, J. Phys. Chem. B **105**, 182 (2001).
[11] Y. Kamotani, S. Ostrach, and A. Pline, Phys. Fluids **6**, 3601 (1994).
[12] B. E. A. Saleh and M. C. Teich, *Fundamentals of Photonics* (Wiley, New York, 1991).
[13] K. Miyakawa, H. Adachi, and Y. Inoue, Appl. Phys. Lett. **84**, 5440 (2004).
[14] H. Adachi, S. Akahoshi, and K. Miyakawa, Phys. Rev. A **75**, 063409 (2007).
[15] Erwin J. G. Peterman, Frederick Gittes, and Christoph F. Schmidt, Biophys. J. **84**, 1308 (2003).
[16] J. Won, T. Inaba, H. Masuhara, H. Fujiwara, K. Sasaki, S. Miyawaki, and S. Sato, Appl. Phys. Lett. **75**, 1506 (1999).